PERGAMON

Electrochimica Acta 47 (2002) 3219–3231

ELECTROCHIMICA Acta

www.elsevier.com/locate/electacta

Bifunctionality in Pt alloy nanocluster electrocatalysts for enhanced methanol oxidation and CO tolerance in PEM fuel cells: electrochemical and in situ synchrotron spectroscopy

Sanjeev Mukerjee *, Richard C. Urian

Department of Chemistry, Northeastern University, 360 Huntington Avenue, Boston, MA 02115-5000, USA

Received 6 December 2001; received in revised form 4 April 2002

Abstract

Electrocatalysis of CO tolerance and direct methanol oxidation on PtMo/C (3:1 a/o) has been investigated in a PEM fuel cell environment. While a 3-fold enhancement is observed for CO tolerance when compared with PtRu/C (1:1), no such enhancement occurred for methanol oxidation. In situ XAS at the Pt L and alloying element K edges for Pt/C, PtRu/C and PtMo/C showed that in contrast to PtRu/C, both Mo and Pt surfaces play a distinct role for CO oxidation. While on the Ru surface there is a competition between oxide formation (from activation of water) and CO adsorption, Mo oxide surface showed no affinity for CO. This provided for efficient CO oxidation at low overpotentials on PtMo/C. However, the corresponding behavior for methanol oxidation showed that Mo oxy-hydroxides were inhibited from efficient removal of CO and CHO species in contrast to Ru oxides. The Mo surface oxides also showed a redox couple involving (V to VI) oxidation states in the presence of both CO and methanol.

Keywords: CO tolerance; In situ XAS; Electrocatalysis; Cancel bifunctionality

1. Introduction

Enhancement of the electrocatalytic activity for the six-electron methanol oxidation reaction (MOR) can be considered as a two step challenge. The first is the initial dehydrogenation step involving the abstraction of the first hydrogen by breaking the C–H bond in methanol. The next two dehydrogenation steps being more facile. The second is the oxidation of the CO and CHO moieties formed on the surface, following the dehydrogenation steps (see reference [1] for a recent review on Direct Methanol Oxidation). The current state of the art electrocatalysts rely on the 'bifunctional approach', in which a second element such as Ru initiates the oxidation of the CO or CHO species by activating water (hence forming surface oxygenated species such as OH) at lower potentials. However, as reported previously [2], a simple model of bifunctionality based on the ability of the more oxidizable alloying component (such as Ru) to activate water and form oxygenated species at lower overpotential, fails to account for the fact that good electrocatalyst for CO tolerance are sometimes poor for methanol oxidation. This has been shown previously for PtSn electrocatalyst [2,3]. At the present moment PtRu remains as the electrocatalyst of choice for direct methanol oxidation, however, in contrast to CO electro-oxidation, supported electrocatalysts have shown limited ability to sustain electrocatalytic activity beyond 0.3 A cm^{-2}. This has necessitated the use of unsupported electrocatalysts with high electrocatalyst loading requirements, which are an order of magnitude higher than the current state of the art low Pt loading electrodes used in Proton Exchange Membrane Fuel Cells (PEMFC).

Recently, Mukerjee et al. [4], showed up to 3-fold enhancement in activity for CO oxidation relative to the current state of the art PtRu/C (1:1 a/o) in a PEMFC

* Corresponding author. Tel.: +1-617-373-2382; fax: +1-617-373-8795

E-mail address: smukerje@lynx.neu.edu (S. Mukerjee).

0013-4686/02/$ - see front matter
PII: S0013-4686(02)00242-6

operating at 85 °C, comparing steady state (half and single cell) polarization data with PtMo/C (8.7:1.3 a/o). Comparisons were based on the steady state PEMFC performance in the presence of 100 ppm of CO in the anodic hydrogen stream. Cyclic voltammograms of PtMo/C without adsorbed CO in both a PEM fuel cell in a half cell configuration at 55 °C as well as at room temperature in a flooded electrode mode with 1 M $HClO_4$ indicated a redox type behavior at 0.45 V versus RHE. Comparison of this redox behavior with the corresponding Mo K edge X-ray absorption near edge spectra (XANES) at 0.0 and 0.54 V indicated a change in the Mo oxidation state. The exact nature of this oxidation state change, however, is yet to be determined. Further, cyclic voltammetric stripping of CO both in a PEM half cell configuration at 55 °C as well as in a flooded electrode configuration at room temperature (with 1 M $HClO_4$) showed two peaks. This is in contrast to a single peak typically observed for PtRu/C under the same conditions. This may indicate that both Mo and Pt atoms which are on the surface have distinct roles for CO oxidation albeit at different potentials. A recent report by Grgur et al. comparing kinetic properties of both bulk and supported PtMo/C electrocatalysts using a rotating thin layer electrode (RTLE) method [5] reported a mismatch based on the alloying compositions. This was ascribed either to a surface segregation phenomenon in the alloy nanocrystals different from those in the bulk or that the alloying with Pt is incomplete and that the alloy nanocrystals are richer in Mo relative to that expected based on the alloying composition in the catalysts. Prior publications by Grgur et al. [6,7], studied electro-oxidation kinetics of H_2, CO and H_2/CO mixture on smooth and well-characterized PtMo surfaces in 0.5 M H_2SO_4 at 60 °C. This study suggested that the oxidation states of Mo surface atoms as well as the nature of Mo surface oxides are determining factors in the electrocatalysis of H_2, CO and H_2/CO mixtures on these alloys. It was suggested that the oxyhydroxide state of Mo (predominantly as $MoO(OH)_2$) is reactive towards the oxidative removal of CO, but this state can also reduce the availability of adjacent Pt surface atoms for the dissociative adsorption of molecular hydrogen. On the other hand, although de-protonated oxides (for example, MoO_3) also have a screening effect on the adjacent Pt surface atoms they are very inactive in a reaction with CO_{ad}. Recently CO tolerance of ball milled PtMo electrocatalysts have been reported [8]. These results did not show any enhancement versus PtRu of corresponding atomic ratio. Ternary alloy compositions with Al and Mg were also reported (such as $Pt_{0.5}Mo_{0.5}Al$ and $Pt_{0.5}Mo_{0.5}Al_4$, and $Pt_{0.5}Mo_{0.5}(MgH_2)$), however, the real Mo content was reported to be significantly lower due to leaching. Stable steady state polarization results were reported at 0.5 V (single cell) and 80 °C. In addition ex-situ XPS analysis showed the presence of Mo in oxidation states of (V) and (VI). A more recent report by Pozio et al. [9], comparing the steady state polarization for hydrogen oxidation reaction (HOR) by PtRu/C and PtMo/C showed similar performances, wherein the a Heyrovsky–Volmer mechanism was proposed to explain any departure from linearity of the E versus i data.

Enhanced activity for methanol oxidation has been recently reported [10] on $Pt/MoO_x/C$ composite electrodes prepared by an electrochemical co-deposition technique using a glassy carbon electrode as a substrate. This study also indicated the possibility of a redox couple involving Mo, the oxidation state changes ascribed to the redox peaks in the voltammogram were a Mo(VI)/Mo(IV) couple. The enhancement for methanol oxidation was ascribed to the existence of this redox couple in the sub-stiochiometric lower valence MoO_x ($2 < x < 3$) and possibility of a proton spillover effect from hydrogen molybdenum bronze. However, it must be emphasized that this report represents results on a composite PtMo system, prepared by electro-deposition, and hence it is very different to the results published earlier [4] on CO tolerance, wherein the formation of PtMo alloy was reported. Contrary to this report, preliminary results reported by us [11], show that PtMo alloys with the atomic composition of (3:1 and 4:1; Pt:Mo ratio) do not exhibit any enhancement of direct methanol oxidation in contrast to their excellent CO tolerance abilities.

In light of these earlier conflicting reports on CO tolerance and direct electrochemical oxidation of methanol, this paper aims to investigate the steady state behavior of PtMo/C electrocatalyst for both cases. Further, correlation will be made with results of in situ XAS measurements at both the Pt L (L_3 and L_2) and the Ru and Mo K edges. The goal is to (a) explain the enhanced CO tolerance capabilities of the PtMo/C alloy system in comparison to Pt/C and PtRu/C (1:1 a/o) and (b) explain their methanol oxidation characteristics in comparison to corresponding data for Pt/C and PtRu/C (1:1 a/o). Application of XAS to study the structure-property relationship of nano-phase bimetallic clusters at an electrochemical interface is described in detail elsewhere [12,13]. Briefly, the near edge region of the XAS, X-ray absorption near edge structure (XANES) examines the changes to the electronic structure (Pt *d-orbital* vacancies etc.). The extended part of the spectra, extended X-ray absorption fine structure (EXAFS) probes the changes to the short range atomic order (primarily, the first shell bond distance and coordination number). The primary advantage being the ability to examine these bimetallic clusters with element specificity under actual in situ electrochemical conditions.

2. Experimental

2.1. Electrocatalysts and electrode specifications

The carbon supported (Vulcan XC-72) PtMo/C electrocatalysts were obtained from ETEK Inc., (a division of De Nora, NA, Somerset, NJ). The nominal compositions as specified by ETEK based on Pt:Mo atomic ratio in the PtMo/C catalysts was 3:1 while the corresponding PtRu/C was 1:1 and the metal loading on carbon was 30 w/o. For control experiments, carbon supported (Vulcan XC 72) Pt/C from ETEK Inc., was used, with the metal loading on carbon being 20 w/o. X-ray diffraction was conducted using the high resolution X18A beam line at the National Synchrotron Light Source (NSLS) at Brookhaven National Laboratory. Previously reported characterization of the 3:1 and 4:1 PtMo/C composition [5] showed the existence of a fcc metallic phase with an average particle size of ca. 4 nm. Since the lattice constants for the PtMo solid solutions are very close to that of pure Pt, the compositions of the nanocrystalline phase could not be determined. Within the limits of this technique, however, no separate phases associated with Mo e.g. metal oxide, or carbide were detected, suggesting thereby that most if not all of the Mo was alloyed with the Pt. TEM analysis of the as-received electrocatalysts were conducted using a JEOL transmission electron spectrometer (model 3010) using an energy of 200 kV. Electron diffraction data were also obtained for every sample. Line broadening analysis of the primary XRD peak $\langle 111 \rangle$ was conducted using the Scherrer treatment of the data. The data were first fitted to an indexing program, which allowed accurate measurement of the line widths at half maximum. These widths were then used to obtain the particle size. Corrections for beam deviations in the instrument were considered negligible due to the high collimation of the synchrotron beam.

Anode electrodes for CO tolerance measurements of steady state polarization in PEM single/half cells were prepared by a brushing/rolling technique developed in-house. They comprised of a carbon cloth substrate (ETEK, Carbon Cloth), with a diffusion layer containing teflonized carbon (35 w/o PTFE) with an average thickness of 35 μm, which was pre-sintered at 320 °C under Ar. The reaction layer comprised of the catalyst (0.4 mg cm^{-2}, Pt or Pt alloy catalyst loading)+ solubilized Nafion® (5 w/o mixture in lower aliphatic alcohols and water, Aldrich, USA). The gas diffusion side of the electrode had a thinner diffusion layer of C/PTFE (30 w/o) of ~15 μm thickness. Membrane electrode assemblies were made with anodes of Pt/C, PtRu/C and PtMo/C while keeping the cathode electrode the same (20% Pt/C, ETEK electrode, 0.4 mg cm^{-2} Pt loading). The Nafion loading in the reaction layer of the electrodes was ~1.9 mg cm^{-2} and the assembly was made by hot pressing at 1000 Kgf cm^{-2}, 140 °C for 3 min. The membrane was Nafion® (115), which was cleaned by a procedure, described in detail elsewhere [14]. The methodology for preparation of the electrodes and membrane electrode assembly for steady state polarization measurements of methanol oxidation is given elsewhere [15]. For DMFC measurements, the same supported electrocatalysts were used as in the case of CO tolerance. The electrode loading was 1 mg cm^{-2} (for both anode and cathode electrodes) in this case and the membrane electrode assemblies were made using a decal method. In this technique, a thin layer of the electrocatalyst (1 mg cm^{-2} loading, 30% metal on carbon) and ionomer (1.9 mg cm^{-2}) was first deposited directly on the membrane by the decal process followed by mechanically pressing a carbon paper (hydrophilic) as a backing layer. The direct methanol oxidation polarization measurements were conducted at NASA-JPL.

Separate sets of electrodes were prepared for in situ XAS measurements, using a methodology described elsewhere [2]. Electrocatalyst loading of ~45 mg cm^{-2} (±3.5) was used based on the absorption cross sections of Pt L_3 and Ru and Mo K edge in order to afford a step height close to 1. The electrodes were first soaked in 1 M $HClO_4$ for 48 h followed by vacuum impregnation, which ensured a totally flooded state. This was important, since XAS for these nano-phase materials (< 50 nm) is a bulk averaging techniques in both transmission and fluorescence modes.

2.2. Steady state polarization and dynamic measurements in a PEM fuel cell

Steady state polarization measurements of CO tolerance were carried out in a fuel cell test station using a cell fixture for a 5 cm^2 membrane-electrode assembly, which allowed for both single and half-cell polarization measurements. The test station was built in-house and had provisions for controlling temperature, pressure, humidification and flow (mass flow) of reactant gases. The bipolar plates made of carbon with resin impregnation (POCO graphite, TX, USA) had conventional ribbed flow channels, the anode chamber contained a built in hydrogen reference electrode with a separate flow channel, which allowed for simultaneous half cell measurements. Details of the fuel cell test station and the single cell test fixture are given elsewhere [14]. Steady state single and half-cell polarization curves were measured as a function of temperature (55–115 °C) and CO/H_2 ratio (0–100 ppm). The respective anode/cathode pressures were maintained to regulate the anode and cathode chambers at 1 atm, based on the cell temperature. The humidification temperatures of the anode and cathode were maintained at 15 and 5 °C, respectively above the cell temperature. For H_2/CO

mixtures, premixed gas cylinders were used (Matheson, NJ).

The anodic half-cell polarization measurements for direct methanol oxidation were conducted at 90 °C, with a methanol flow rate of 2 l min^{-1} and a cathode backpressure of 20 psig. Details of the measurement conditions and test station are given elsewhere [15]. Anode half-cell polarization studies were performed by methodologies described in detail elsewhere [15].

Cyclic voltammetry was carried out using the same single cell set-up at 55 °C. To investigate the voltammetric stripping of CO, H_2 containing 100 ppm of CO was passed through the working electrode (anode side) for at least 1 h while maintaining a constant potential (0.05 V vs. RHE). At the same time pure hydrogen was passed through the counter and reference electrode compartments. Prior to voltammetric stripping of CO, the working electrode (anode side) compartment was purged with N_2 for about 30 min to remove residual H_2 gas and non-adsorbed CO. Cyclic voltammetry was also conducted at room temperature in a spectro-electrochemical cell used for XAS analysis. The electrodes, in a completely flooded configuration were cycled both in the presence and absence of CO in 1 M $HClO_4$ using the in situ XAS cell. For CO stripping voltammetry, pure CO (Matheson, NJ) was purged close to the working electrode for 1 h with the electrode polarized at 0.0 V versus RHE in a fume hood. The electrode was then purged with pure N_2 for 30 min followed by voltammetric stripping. Similarly cyclic voltammetry was conducted in the presence of methanol (1 M $HClO_4$ + 0.3 M MeOH) in a flooded mode using the in situ XAS cell at room temperature. All cyclic voltammetric experiments were conducted at 5 mV s^{-1}.

2.3. XAS measurements

XAS measurements were conducted at beam line X11A at the NSLS in Brookhaven National Laboratory, with the storage ring operating at 2.8 GeV and a current between 350 and 120 mA. Data were collected at both the Pt L (L_3 and L_2) and the Ru and Mo K edges in the transmission mode using a three detector set up (incident, transmitted and a reference). The reference detector provided accurate calibration and alignment of the edge positions, for which a pure standard foil ($\mu x = 1$) of the element edge being probed was employed. Details of the beam line optics, and monochromator are given elsewhere [16]. The monochromator, (Si 111 crystals) was detuned by 15% for the Pt L edge and 10% for the Mo and Ru K edges, respectively, to reject higher harmonics. All measurements were carried out in an in situ spectro-electrochemical cell, which allowed XAS measurements in the transmission mode with the working electrode in a totally flooded state. Two types of in situ cells were used in this study. For investigations on the effect of adsorbed CO, a cell with arrangements for bubbling gas close to the working electrode was used. Details of this spectro-electrochemical cell is given elsewhere [17]. For studies in 1 M $HClO_4$ with and without 0.3 M MeOH a sealed compression cell was used, details of which are given in [12,13].

The methodology for the XANES data analysis followed the procedure described by Wong et al. [18]. The methodology used to determine the Pt 5 d-orbital vacancies is based on earlier work by Mansour et al. [19,20]. EXAFS analysis involved algorithms developed by Koningsberger and co-workers [21,22]. Detailed EXAFS analysis was carried out on the Pt L_3 and Ru and Mo K edge data. The methodology used for the analysis followed those reported previously [12,13,16]. The phase and amplitude parameters of the sample data were fitted to those derived from experimental and theoretical standards. In the case of the Pt L_3 edge data, the standards for Pt–Pt and Pt–O interactions were experimentally obtained from Pt foil and $Na_2Pt(OH)_6$ data at liquid N_2 temperature. For the Pt–Mo and Pt–Ru interactions, the corresponding phase and amplitude parameters were obtained from theoretical standards calculated with FEFF6 program using a model fcc structure. In these model structures, appropriate changes were made to account for the variation of the atomic ratios in the different PtMo alloy compositions.

In situ EXAFS data at the Pt L (L_3 and L_2) and the Ru and Mo K edges were taken at 0.54 V using a computer interfaced potentiostat/galvanostat (Autolab, PGSTAT 30). The electrolyte of choice was 1 M $HClO_4$. Prior to acquiring in situ EXAFS data the electrode was cycled between 0.0 and 0.65 V at least 25 times, the low 0.65 V upper voltage cutoff was used to avoid any possible dissolution of Mo from the electrode surface. Since the purpose of the EXAFS analysis in this investigation was to investigate the effect of alloying Mo to Pt in the nano-phase PtMo/C electrocatalysts and compare it to the analogous data from PtRu/C and Pt/C. Detailed EXAFS analysis is reported at 0.54 V. Data at this potential were devoid of any effects of surface adsorbed species being in the double layer region and close to the potential of zero charge.

In all fits, Gaussian pair distribution functions (PDF) for the Pt–Pt and Pt–M (M = Ru or Mo) pairs were sufficient to model the EXAFS spectra. The effect of an harmonic thermal vibrations and symmetric interatomic pair distribution functions, which can potentially cause an under estimation of the coordination numbers were checked by using cumulant expansion algorithms. These were done by using asymmetrical PDF by including the third and fourth terms in the cumulant expansion as fitting parameters. Upon using the asymmetric PDF, the coordination numbers and disorders on the average increased by 12 ± 5 and $18 \pm 9\%$ for PtMo/C (3:1) {a representative example} and for Pt–Pt and Pt–

Mo interactions, respectively, relative to those obtained using Gaussian PDF. The observed invariance in the coordination numbers and disorders were random in nature and showed no correlation with the PtMo ratio. For bond distances, on the average, the Pt–Pt and Pt–Mo interactions increased by 0.02 ± 0.001 and 0.03 ± 0.002 Å, respectively, relative to those obtained using Gaussian PDF. Overall, the effect of asymmetry on the coordination number, disorder and distance was close to negligible. Hence, hereafter, the results reported are those obtained using Gaussian PDF.

3. Results and discussion

3.1. Characterization of the nanocluster size and morphology: powder XRD, TEM and in situ XAS measurements

Detailed characterization of the nanocluster size and morphology are essential for understanding the true importance of the electrochemical data. A representative TEM picture of the PtMo/C (3:1 a/o) from ETEK is shown in Fig. 1. The corresponding electron diffraction pattern is also shown. Analysis of the TEM pictures for other electrocatalysts in terms of their particle size is given in Table 1. The average particle size obtained from TEM analysis ranges between 30 and 35 Å. The dispersion of the electrocatalysts was excellent with a very narrow distribution of particle size (within 15 Å for all the electrocatalysts). XRD analysis of the electrocatalysts showed a very high degree of crystallinity. Fits of the XRD data to an indexing routine showed that all of the patterns (Pt and Pt alloys) corresponded to a fcc lattice. The lattice parameters obtained are given in Table 1. In addition, the Pt–Pt bond distances based on a fcc lattice were calculated (Table 1). As evident from the data, alloying of Pt with Ru and Mo results in a lowering of the lattice parameters (and hence the Pt–Pt bond distance). While the perturbation of the lattice parameter for PtMo was negligible, those for PtRu/C were significant. Here the Pt–Pt bond distance is lowered by ca. 0.026 Å. As pointed out in the Section 2, the XRD pattern for PtMo/C was very close to that of Pt/C, hence a strong conclusion on alloy formation was not possible. As shown in Table 1, the lattice parameters were very close to that for Pt/C, hence negligible change in the Pt–Pt bond distance as compared with Pt/C. The electron diffraction patterns for Pt and PtMo/C were also very close. The particle size obtained using the $\langle 111 \rangle$ diffraction line broadening analysis showed remarkable agreement with the corresponding data from TEM. The particle size obtained were all in the range of 28–35 Å. Using a cubo-octahedron cluster model [23], the number of surface sites as compared with the bulk is ca. 25%. This is significant in light of the use of in situ XAS to investigate surface processes, as the spectroscopy in transmission mode is a bulk average.

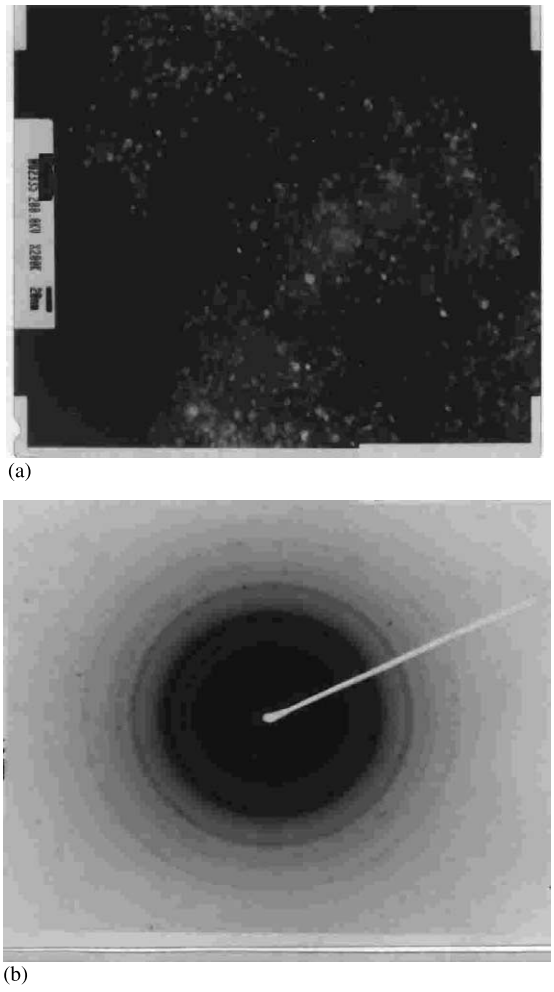
(a)

(b)

Fig. 1. (a) TEM image and (b) electron diffraction pattern for PtMo/C (3:1 a/o) electrocatalyst (as received).

3.2. Electrochemical characterization: dynamic and steady state measurements

Fig. 2 shows the steady state single and half cell (inset) polarization plots at 85 °C, comparing performance for Pt/C, PtRu/C and PtMo/C (3:1 a/o) as anode electrodes (cathode: Pt/C, 0.4 mg cm^{-2}) in H_2/CO [100 ppm]//O_2. Representative data for a Pt/C anode electrode without CO under the same conditions is included. The respective anode/cathode pressures were 16/11 psig at 100/90 °C, respectively, to maintain a constant water vapor pressure of 1 atm. As evident from the electrode performance data, PtMo/C (3:1 a/o) exhibits a significantly higher CO tolerance as compared to the current state of the art PtRu/C (1:1 a/o). Half-cell anode polarization data with H_2/O_2 under the same conditions showed negligible differences (not shown). This lack of variation in the H_2/O_2 anode polarization is consistent

Table 1
Results of XRD and TEM analysis of carbon supported Pt/C, PtRu/C and PtMo/C electrocatalysts

Electrocatalyst	XRD analysis		Nominal atomic ratio (a/o) [metal loading/C] (%)	Particle size (Å)	
	XRD lattice parameter (Å)	Pt–Pt bond distance (Å)		X-ray line broadening analysis	TEM
Pt/C	3.927	2.777	– [20%]	28	30
PtRu/C	3.8905	2.751	1:1 [30%]	35	35
PtMo/C	3.9145	2.768	3:1 [30%]	31	31

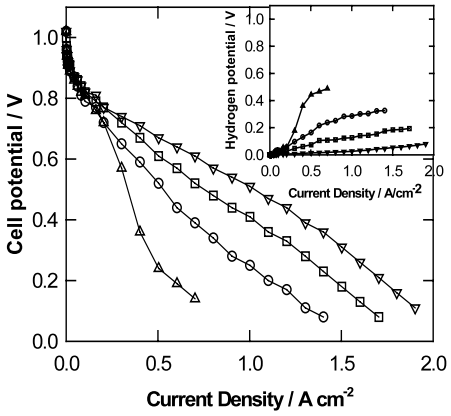

Fig. 2. Steady state polarization measurement in a 5 cm^2 PEMFC single/half cell set up. Cell operating conditions were 85 °C, back-pressure 16 and 11 psig, humidification temperature 100 and 90 °C for anode and cathode, respectively. Cathode electrode: Pt/C, 20% on C, 0.4 mg cm^{-2} Pt loading. Anode electrodes, Pt/C (△), PtRu/C (1:1) (○), PtMo/C (3:1) (□) with H_2[100ppm of CO]/O_2. Performance of a Pt/C control experiment without CO (▽) is also included for reference. Inset in the figure shows the corresponding half-cell anodic polarization curves.

with previous data [24], which compared the steady state anode polarization behavior of similar nano-dispersed Pt and alloys of Pt with the first row transition series ranging from Cr to Ni. Detailed analysis of the electrode kinetic data in this previous study [24], including comparison of the activation energies indicated negligible differences in the activity for hydrogen oxidation as a consequence of alloying. Hence the differences in the single cell polarization are almost entirely due to differences in the electrocatalytic activity for CO oxidation on the different electrocatalyst surfaces as shown in the half-cell polarization data in the inset of Fig. 2. Comparison of the specific current densities (mA cm^{-2} g) at 100 and 50 mV obtained from the iR corrected anode half-cell polarization plots indicate ca. 3-fold enhancement in activity for the PtMo/C compared with the PtRu/C electrocatalyst (Table 2). It is interesting to note that in contrast to Pt/C, the alloy electrocatalysts do not exhibit a classical limiting current behavior, clearly indicating a different oxidation mechanism in the mixed H_2/CO environment.

The differences in the polarization behavior in the presence of CO on the various catalysts can be analyzed by taking into account the Tafel–Volmer mechanism for the HOR in an acid media [25].

$$H_2 + 2S \rightarrow 2S\text{–}H \quad \text{(Tafel)} \quad \text{(I)}$$

$$S\text{–}H \rightarrow S + H^+ + e^- \quad \text{(Volmer)} \quad \text{(II)}$$

here, S represents an active site on the electrocatalyst surface.

In the absence of CO, the Tafel slopes are in the range of 20–30 mV per decade for all the electrocatalysts. This, according to the above mechanism, implies that both steps (I) and (II) progress very fast corresponding to a very large exchange current density. In the presence of CO, there is a large fraction of the surface covered with CO, resulting in step (I) becoming rate limiting at higher overpotentials (<50 mV, or above 100 mA cm^{-2}). However, at lower overpotentials (>50 mV), there remains sufficient coverage of H to allow step (II) to progress very fast, hence resulting in a Tafel slope of 20–30 mV per decade (Fig. 4(b)). At higher overpotentials, when step (I) approaches a limiting behavior, the current density is controlled by the rate of H adsorption and a limiting current is observed in the polarization plot. This is particularly applicable for the case of Pt/C (till >90 °C) and PtRu/C (>55 °C) as reported previously [26], wherein the Tafel slope $\rightarrow \infty$. However, at 85 °C in the presence of 100 ppm of CO, both PtRu/C and PtMo/C show a quasi-limiting behavior, thereby indicating the ability to prevent complete coverage by CO on the surface, and/or the ability to oxidize CO at lower overpotentials. Steady state anode polarization measurements in a DMFC, are shown in Fig. 3 as an iR corrected plot. These data clearly demonstrate that the corresponding enhancement of MeOH oxidation does not occur with PtMo/C as seen earlier with CO tolerance (Fig. 2). Comparison of the overpotential at 100 mA cm^{-2} shows that PtMo/C performs very close to Pt/C and that PtRu/C is significantly better. This is also true for the comparison of the limiting currents (Table 2). This clearly demonstrates the fact that a simple extrapolation of the bifunctional behavior does not apply for all electrocatalysts. As pointed out in the Section 1, the mechan-

Table 2
Electrode kinetic parameters

Electrocatalyst	Limiting current (i_L) (mA cm^{-2})	Tafel slope, b (mV per decade)	η @ 100 mA cm^{-2} (V)
For methanol oxidation at 90 °C with 1 M MeOH and Nafion 117 membrane [a]			
Pt/C	591	180	0.45
PtMo/C	572	183	0.44
PtRu/C	635	224	0.3
Electrocatalyst	Current density at 100 mV $I_{100\ mV}$ (mA cm^{-2})	Current density at 50 mV $I_{50\ mV}$ (mA cm^{-2})	
For CO tolerance H_2 [100 ppm of CO]/O_2 at 85 °C based on steady state anode polarization in a 5 cm^2 PEMFC			
Pt/C	230	162	
PtRu/C	310	175	
PtMo/C	800	550	

[a] Electrode loading was 4 mg cm^{-2} anode and cathode.

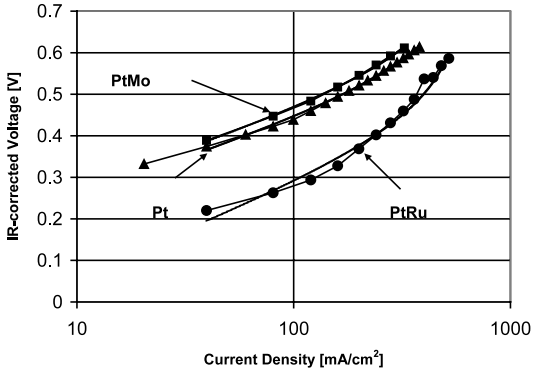

Fig. 3. iR corrected steady state half cell polarization plots for methanol oxidation (1 M MeOH) at 90 °C, Nafion 117, electrode loading 4 mg cm^{-2}, anode and cathode. Pt/C (▲), PtRu/C (●) and PtMo/C (■).

ism for direct MeOH oxidation has two possible rate limiting steps (a) the initial abstraction of the C–H bond and the adsorption of the methanolic species and (b) the eventual oxidation of CO species. On Pt/C the overwhelming evidence points to (b) being the rate limiting step, while as pointed out by Gasteiger et al., and others [3], on PtRu/C (1:1) it could be step (a).

Cyclic voltammograms for PtMo/C in 1 M $HClO_4$ in the in situ spectro-electrochemical cell at ambient temperature (25 °C) in the flooded electrode mode are presented in Fig. 4(a). The results obtained under similar conditions, after a CO purge for 1 h (electrode polarized at 0.0 V), of Pt/C and PtMo/C are presented in Fig. 4(b) in a PEMFC at 55 °C. Results for PtMo/C in the absence of CO (Fig. 4(a) and (b)) shows evidences of both Pt and Mo features although the Pt–H_{upd} region is not as defined as the Pt/C or PtRu/C electrodes. However, the Pt–H feature is evident from the peak for hydrogen desorption for the electrode polarized at 0.0 V (N_2 purge) for 1 h (Fig. 4(b)). As in the case of the bulk alloy [5], voltammogram of PtMo/C in the absence of CO, shows a redox behavior in the potential range of 0.43–0.50 V versus RHE which can be attributed to Mo.

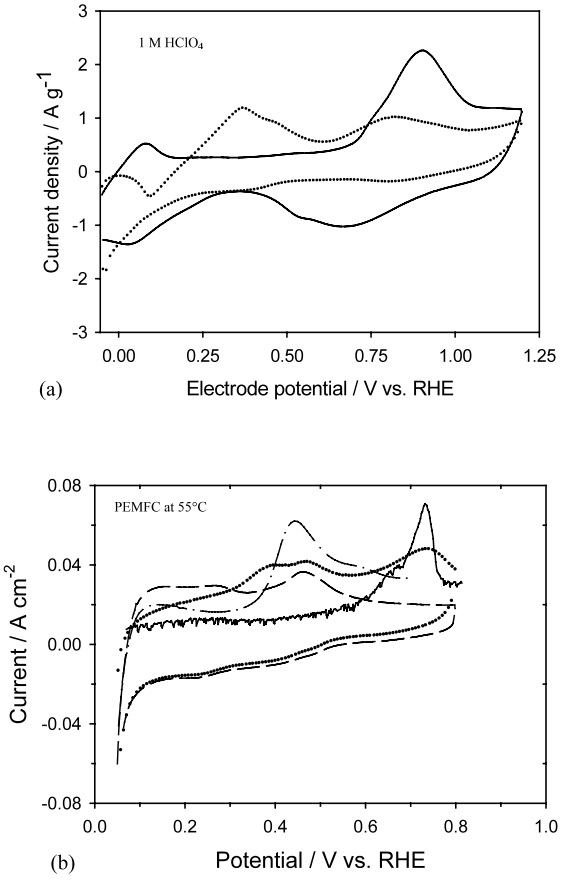

Fig. 4. Cyclic voltammograms in (a) flooded electrode (1 M $HClO_4$, XAS cell) and (b) in a PEMFC with a 5 cm^2 membrane electrode assembly at 55 °C with cathode, Pt/C and anode PtMo/C [CO purge, 1 h] (···); PtMo/C [N_2, purge, 1 h] (---); PtRu/C [CO purge, 1 h] (— · — · —); and Pt/C [CO purge, 1 h] (—).

Comparison with the Pourbaix diagram for Mo indicates that this redox behavior is most likely due to a $Mo^{4+} \leftrightarrow Mo^{6+}$ oxidation state change. Repeated cycling between 0.05 and 1.2 V for 50 cycles showed no changes indicating minimal dissolution of Mo from these electrocatalysts. It will be later shown that this oxidation state change is actually a $Mo^{5+} \leftrightarrow Mo^{6+}$.

Experiments in the liquid acid electrolyte in the presence of adsorbed and dissolved CO (Fig. 4(a)), and in the PEM environment (Fig. 4(b)) seem to indicate that both Pt and Mo are active for the CO oxidation. CO oxidation is first initiated at lower potentials by oxygenated species on the Mo surface at ca. 0.05 V, followed by Pt above 0.55 V. Comparison of the corresponding voltammogram for Pt/C confirms the CO oxidation beyond 0.55 V is due to Pt. The presence of two distinct peaks is significant, in that it is in complete contrast to the corresponding voltammetric response from electrocatalysts such as PtRu/C and PtSn/C. This indicates a unique role for Mo in these electrocatalysts because it exhibits a more complex behavior as compared to predictions based on the 'bifunctional mechanism', where the oxides on the more oxidizable element provide the necessary oxygenated species for the CO oxidation on Pt.

3.3. *In situ XAS results at Pt L edge*

The ratio of Pt to Mo atoms and Pt to Ru atoms in the electrocatalysts was determined from the edge jumps at the Pt L_3, and the Ru and Mo K edges using a methodology described elsewhere [24]. The results obtained indicated 72.5 a/o Pt for PtMo/C 3:1 and 48 a/o Pt for PtRu/C (1:1). Fig. 5(a) shows the comparison of the forward Fourier transforms (k^3 weighted) for Pt/C and PtMo/C (3:1) after correcting for phase shifts. Comparison of these phase corrected Fourier transforms clearly indicate the presence of both Pt–Pt and Pt–Mo interactions in carbon supported PtMo clusters. Detailed EXAFS analysis was conducted according to the procedure described in detail in the Section 2. For this, forward and inverse Fourier transforms were obtained using windows, which are described as a footnote below Table 3. All fits were carried out as iterative least square fits. The approach taken in fitting was to choose the simplest model first and attempt to get unique solutions to the fits. Thus for EXAFS at the Pt L_3 edge for Pt/C at 0.54 V, it was possible to fit the data to a single shell Pt-Pt interaction. For PtRu/C and PtMo/C data at the Pt L_3 edge taken at 0.54 V, a two shell fit with Pt–Pt and Pt–M interactions were required. The Pt–M interactions (Pt–Ru and PtMo) were generated theoretically as mentioned in the Section 2. For this FEFF software (version 6) of Rehr et. al. [27] was used with cartesian coordinate inputs for a fcc lattice. Table 3 shows the results of these EXAFS analysis at the Pt L_3 edge in 1 M $HClO_4$ for Pt/C, PtRu/C (1:1 a/o) and PtMo/C (3:1) for data collected at 0.54 V. In addition, the results of the XANES analysis at the Pt L_3 and L_2 edge using methodologies described in the Section 2, is included in Table 3. These results indicate that PtMo/C is an alloy. This is evident from the increase of the Pt d-band vacancy/atom for Pt

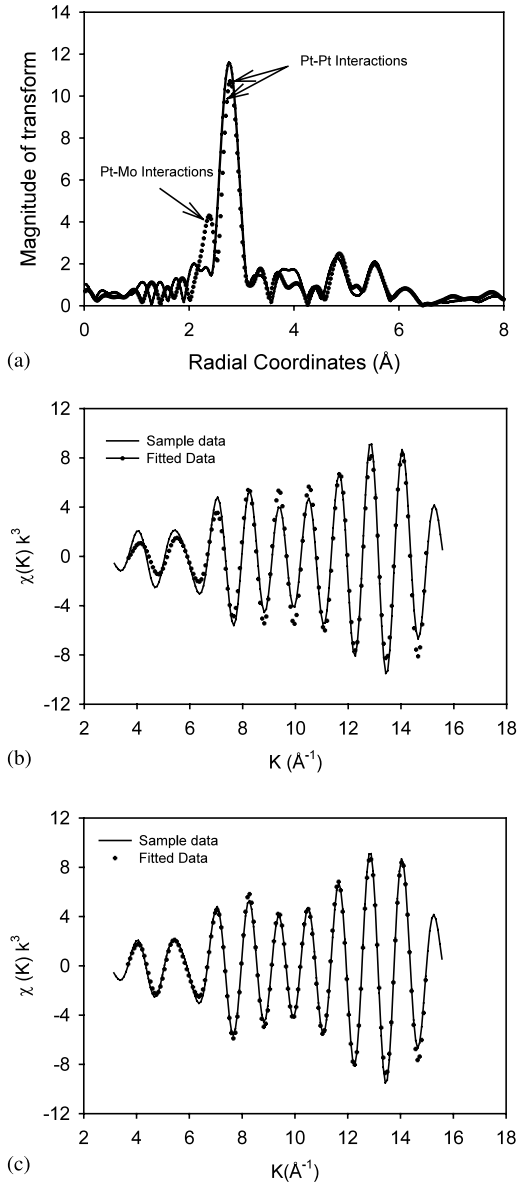

Fig. 5. Analysis of XAS at the Pt L_3 edge for Pt/C and PtMo/C (3:1) collected at 0.54 V vs. RHE in1 M $HClO_4$. (a) Comparison of the forward Fourier transform of the EXAFS after correction for phase shifts. (b) Comparison of the fits in K-space for PtMo/C, k^3 weighted, taking single shell Pt–Pt interactions only and (c) a two shell fit in K-space, k^3 weighted with Pt–Pt and Pt–Mo interactions.

alloyed to Mo and the lowering of the Pt–Pt bond distances. However, both these parameters are perturbed to a much higher degree in the case of PtRu/C. In addition the coordination numbers (a sum of the Pt–Pt and Pt–M CN's for the alloys) are in good agreement with those expected from the particle sizes obtained from TEM and XRD analysis. This is based on a cubo-octahedron cluster model described by algorithms of Benfield [23]. Fits in K-space (k^3 weighted), both as a single shell fit (Pt–Pt interactions) and as a two shell fit (Pt–Pt and Pt–Mo interactions) are shown in Fig. 5(b) and (c), respectively. The quality of the fit in the K-space

Table 3
Results of XANES and EXAFS analysis for carbon supported Pt and Pt alloys (PtRu/C and PtMo/C) at the Pt L edge at 0.54 V vs. RHE

Electrocatalyst	Pt d-band vacancy/atom	Shell	EXAFS parameters			
			N	R (Å)	$\Delta\sigma^2$ (Å^2)	ΔE_0 (eV)
Pt/C	0.329					
		Pt–Pt	10.05	2.773	0.0073	−0.67
PtRu/C	0.382	Pt–Pt	7.52	2.73	0.0052	2.07
		Pt–Ru	2.61	2.69	0.0028	−6.24
PtMo/C	0.365	Pt–Pt	9.87	2.76	0.0065	4.56
		Pt–Mo	0.94	2.70	0.0035	−6.78

The windows for the forward and inverse Fourier transforms are given as follows. Fourier transform parameters used to analyze the Pt L_3 EXAFS: Pt/C: $k^n = 3$; Δk (Å^{-1}) = 2.8–14.7; Δr (Å) = 1.38–3.3. PtRu/C: $k^n = 3$; Δk (Å^{-1}) = 2.65–13.8; Δr (Å) = 1.36–3.5. PtMo/C: $k^n = 3$; Δk (Å^{-1}) = 2.7–13.56; Δr (Å) = 1.35–3.45.

clearly shows that PtMo possesses a two shell interaction and is an alloy.

Fig. 6 shows the XANES at the Pt L_3 edge for PtMo/C (Fig. 6(a)) and PtRu/C (Fig. 6(b)) in 1 M $HClO_4$ at 0.54 and 0.9 V versus RHE. At 0.54 V in a sealed electrochemical cell represents a potential close to the double layer region, where no anionic adsorption is expected. Prior reports [12,13,16] have shown this to be true in the presence of 1 M $HClO_4$, where the anionic adsorption from the electrolyte is minimal, a situation similar to perfluorinated sulfonic acids in the PEM membrane. However, 0.9 V is well beyond the potential where the activation of water to give Pt–OH occurs on a pure Pt surface. Prior reports have shown that in the case of PtRu/C this activation step is shifted positive [16]. This is also seen here (Fig. 6(b)), where there is no change in the magnitude of the Pt L_3 white line when comparing the spectra at 0.54 and 0.9 V. However in the case of PtMo/C, the Pt L_3 edge XANES clearly shows increased magnitude of the 0.9 V spectrum, thereby indicating that the activation of water in the aqueous acid solution occurs on the Pt surface in PtMo/C (3:1 a/o) to give Pt–OH on the surface. This has a profound consequence on the electrocatalysis for CO tolerance by PtMo/C, where two CO stripping peaks are observed in contrast to one for PtRu. The second peak at around 0.8 V which can be seen in the cyclic voltammograms (Fig. 4) for CO stripping on PtMo/C is therefore, most likely due to the presence of oxides on the Pt surface. In contrast, the CO stripping on PtRu/C is mostly due to the presence of oxides on the Ru surface. This is direct spectroscopic proof of what was observed using cyclic voltammograms. Fig. 7, shows the XANES spectra at the Pt L_3 edge for PtMo/C and PtRu/C with and without adsorbed CO in 1 M $HClO_4$ at 0.0 V versus RHE. As evident from the spectra, the presence of CO on the Pt surface is clearly apparent for both electrocatalyst cases. The presence of CO on the Pt surface on Pt/C, PtRu/C and PtMo/C is expected based on the wealth of prior data on CO adsorption.

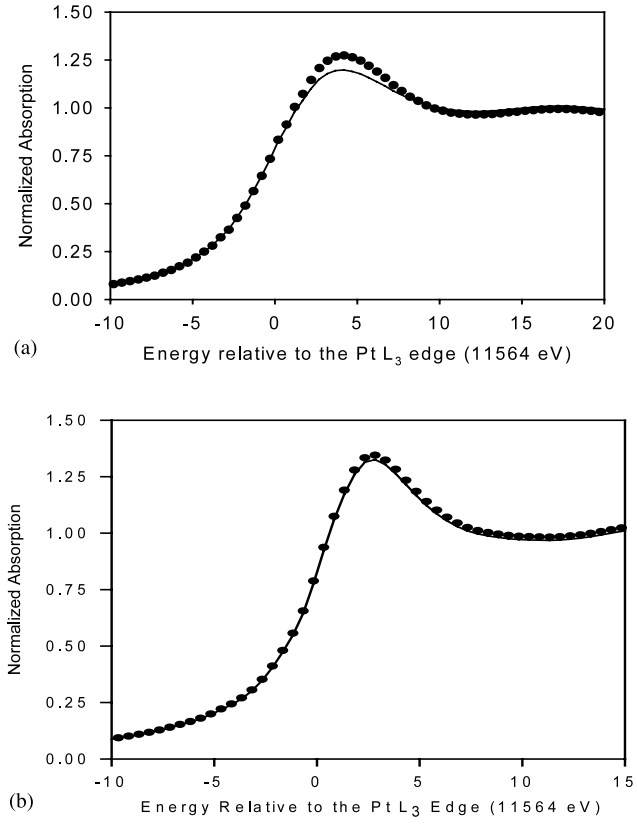

Fig. 6. In situ XANES at the Pt L_3 edge for (a) PtMo/C (3:1 a/o) and (b) PtRu/C (1:1 a/o) in 1 M $HClO_4$ at 0.54 (—) and 0.9 V (●) vs. RHE.

Fig. 8 shows the representative plot of XANES and the corresponding Fourier transform of the EXAFS at the Pt L_3 edge for Pt/C in 1 M $HClO_4$+0.3 M MeOH. XANES at 0.0 V shows a slight reduction in the white line near 0.0 V and a slight widening at the higher energy side (5–10 eV above the edge) relative to the Pt foil standard, indicating the effect of adsorption of methanolic species at this potential and the suppression of hydrogen adsorption. Prior study using electrochemical mass spectrometry [28] and electrochemical quartz crystal microbalance studies [29] have reported such an adsorption effect at this potential. At 0.54 V, there is a

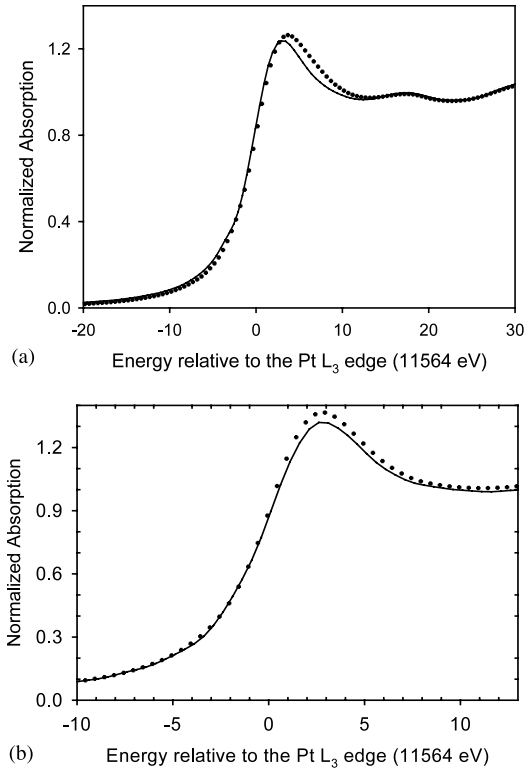

Fig. 7. In situ XANES at the Pt L_3 edge for (a) PtMo/C (3:1 a/o) and (b) PtRu/C (1:1 a/o), at 0.0 V vs. RHE with (···) and without (—) CO purge.

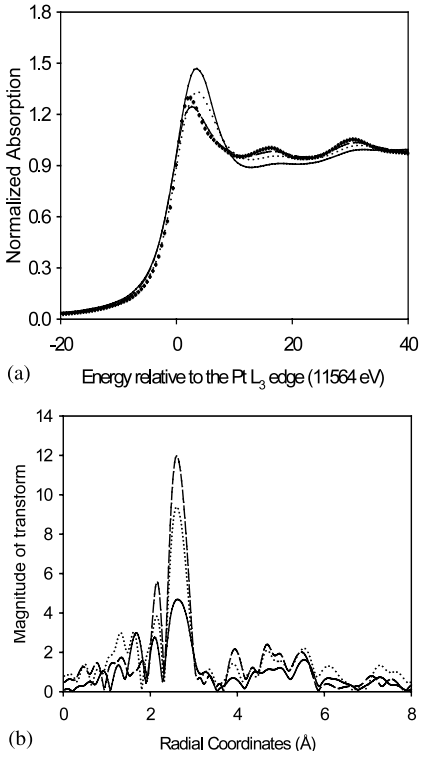

Fig. 8. XAS at the Pt L_3 edge for Pt/C in 1 M $HClO_4$+0.3 M MeOH at 0.0 (---), 0.54 (···), 0.84 V (—) together with data for a Pt reference foil (+) (a) XANES and (b) EXAFS.

significant increase in the white line intensity and broadening at the higher energy side of the spectrum. This is in contrast to the spectra in 1 M $HClO_4$ without methanol, which follows exactly as the Pt foil (as shown before [12,13]). The Pt L_3 XANES with CO adsorbed on Pt/C at 0.0 V in 1 M $HClO_4$ (shown before see reference [30]) compares well with that for Pt/C in 1 M $HClO_4$+ 0.3 M CH_3OH, at 0.54 V showing thereby that for Pt/C there is a build up of CO on the Pt surface at 0.54 V under conditions of methanol oxidation. At 0.84 V, the onset of adsorption by oxygenated species (Fig. 8) becomes evident, similar to the situation without methanol [12]. The corresponding Fourier transforms of the EXAFS at the Pt L_3 edge for Pt/C in the presence of CH_3OH reflect those seen in XANES (Fig. 8). At 0.54 V there is a lowering of the Pt–Pt interactions due to Pt–C interactions and the emergence of two peaks (Pt–Pt and Pt–C interactions) below 2 Å. These peaks are similar to those seen for Pt/C with adsorbed CO (as shown before in reference [30]).

Fig. 9 summarizes the results of XANES analysis for PtRu/C (1:1 a/o) and PtMo/C (3:1 a/o) in 1 M $HClO_4$+ 0.3 M MeOH as a function of potential (V vs. RHE). Here the Pt d-band vacancy/atom is plotted versus electrode potential. As evident from the figure, for PtRu/C, there is an initial increase of the d-band vacancies up to 0.24 V followed by a steady decline at higher potentials. Comparison with the previously published data on changes to the Pt d-band vacancy/atom for PtRu/C [16,30] in 1 M $HClO_4$, shows that the initial increase is due to formation of C_1 oxide species (CO or CHO type species) on the surface following the initial adsorption of the methanolic species at 0.0 V. This build up, however, quickly dissipates after 0.24 V, most probably due to the oxidation by the oxy-hydroxide on the Ru surface. In the case of PtMo/C, however, the Pt d-band vacancies increase steadily till 0.6 V (Fig. 9). This shows that in contrast to Ru, the C_1 oxide species such as CO or CHO are not being removed

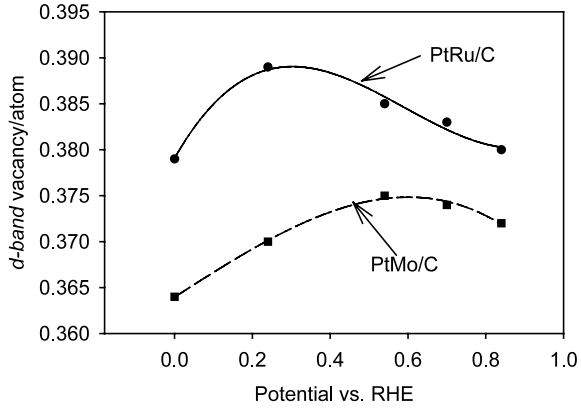

Fig. 9. Pt d-band vacancy/atom obtained from XANES analysis at the Pt L edge for PtRu/C (●) and PtMo/C (■) as a function of electrode potential in 1 M $HClO_4$+0.3 M MeOH.

by the oxy-hydroxides of Mo. This is indeed in contrast to its corresponding behavior with CO. Beyond 0.7 V, the d-band vacancies show a lowering trend, which could be due to formation of Pt–OH on the surface due to activation of water in the aqueous acid on the Pt surface. This has been previously shown to be true in the analysis of Fig. 6. In the case of PtMo/C, therefore, beyond 0.7 V, the removal of CO species appears to be due to oxides on Pt formed as a result of water activation.

3.4. In situ XAS at the Mo and Ru K edge

Fig. 10(a) shows XANES at the Mo K edge for PtMo/C at 0.0 V versus RHE with and without adsorbed CO. As evident from the comparison, there is no perturbation of the white line due to the presence of CO, which indicates that CO has no affinity to the Mo oxy-hydroxide surface. This fact has been previously alluded to by Grgur et al., using rotating disk electrode studies on bulk and dispersed Mo surfaces [6,7]. Fig. 10(b) shows the corresponding XANES plot at the Ru K edge for PtRu/C (1:1 a/o) with and without adsorbed CO at 0.0 V versus RHE. This comparison, however, clearly indicates the presence of adsorbed CO on the oxy-hydroxides of Ru. This is in agreement to a prior report by Gasteiger et. al. on PtRu/C (1:1 a/o) using electrochemical rotating disk experiments [31] on bulk PtRu electrodes. Data at 1.14 V in 1 M $HClO_4$ are also included. As evident from this, potential excursions to 1.14 V result in corrosion and dissolution of Ru from the surface. This is evident from the increased white line and the loss of features in the XANES, typical of a dissolution process.

Fig. 11(a) shows the Ru K edge XANES in 1 M $HClO_4$, as a function of electrode potential (V vs. RHE). Here the magnitude of the white line at Ru K edge shows a steady increase with potential, which indicates that there is a build up of surface oxide species with potential. This build up of surface oxides is responsible for the oxidation of surface CO as well as C_1 oxide species on the surface during the direct oxidation of methanol. Fig. 11(b) shows the corresponding XANES plot at the Ru K edge in the presence of methanol (1 M $HClO_4$+0.3 M MeOH). Here there is a corresponding increase of the white line with an increased electrode potential, which could be due to a combined effect of increased build up of oxy-hydroxides as well as adsorption of C_1 oxide species (such as CO and CHO). It is interesting to note that in contrast to Fig. 11(a) (spectra in 1 M $HClO_4$) where there is a steady increase of the Ru white line with potential, in the presence of MeOH, the white line decreases beyond 0.8 V. This decrease in the white line could be the result of a decrease in the

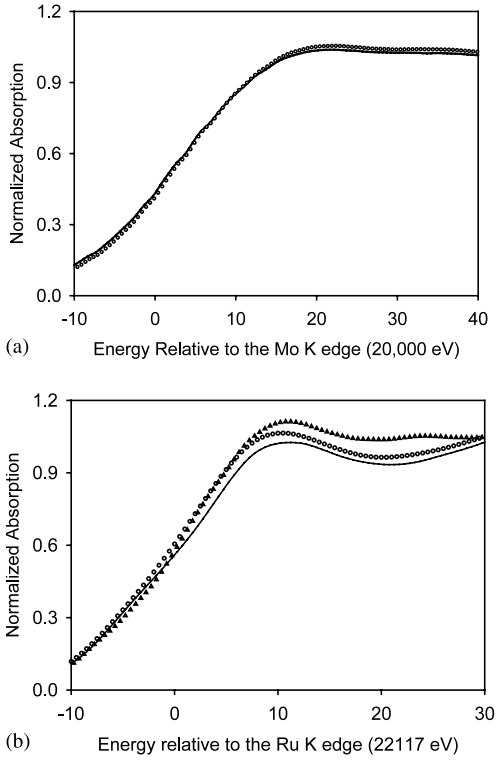

Fig. 10. XANES at (a) Mo K edge for PtMo/C (3:1 a/o) with (○) and without CO (—) at 0.0 V vs. RHE and (b) Ru K edge with (○) and without CO (—) at 0.0 V. Data for PtRu/C at 1.14 V (without CO) (△) are also included.

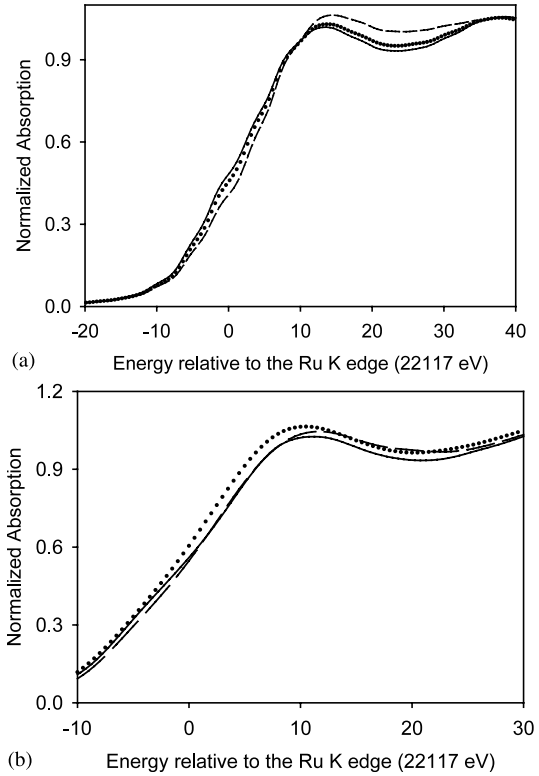

Fig. 11. XANES at the Ru K edge for PtRu/C in (a) 1 M $HClO_4$ and (b) 1 M $HClO_4$+0.3 M MeOH at 0.0 (—), 0.54 (···) and 0.84 (---) V vs. RHE.

abundance of Ru oxy-hydroxides at this potential when in the presence of methanol. This is a subject of a separate investigation.

Fig. 12 shows the Mo K edge XANES at 0.0 and 0.54 V in 1 M $HClO_4$ and for a Mo foil reference standard. As evident from the spectra, Mo in PtMo/C is oxidized with the edge positions shifted positive to the Mo reference foil at potentials as low as 0.0 V. Preliminary analysis of the spectrum with known standards indicate an oxidation state of (+V) at potentials as low as 0.0 V. This suggests its presence in the electrocatalyst as some sort of a hydrated oxide close to $MoO(OH)_2$. Comparison of the spectra at 0.0 and 0.54 V shows a change in the oxidation state from V to VI (Fig. 12(b)), which corresponds to the redox couple observed in the cyclic voltammograms (Fig. 4). These changes in the oxidation state were reversible. This preliminary analysis indicates that, most probably, $MoO(OH)_2$ is present on the surface of the alloy catalyst and it is the active species for the oxidation of CO especially at low electrode potentials. The corresponding XANES at the Mo K edge for PtMo/C in 1 M $HClO_4$+0.3 M MeOH shows that the spectrum is the same between 0.0 and 0.24 V. It then undergoes an oxidation state change at 0.54 V, beyond which at 0.85 V the spectrum remains the same. There is therefore, no additional effect on the Mo K edge XANES due to the oxidation of MeOH.

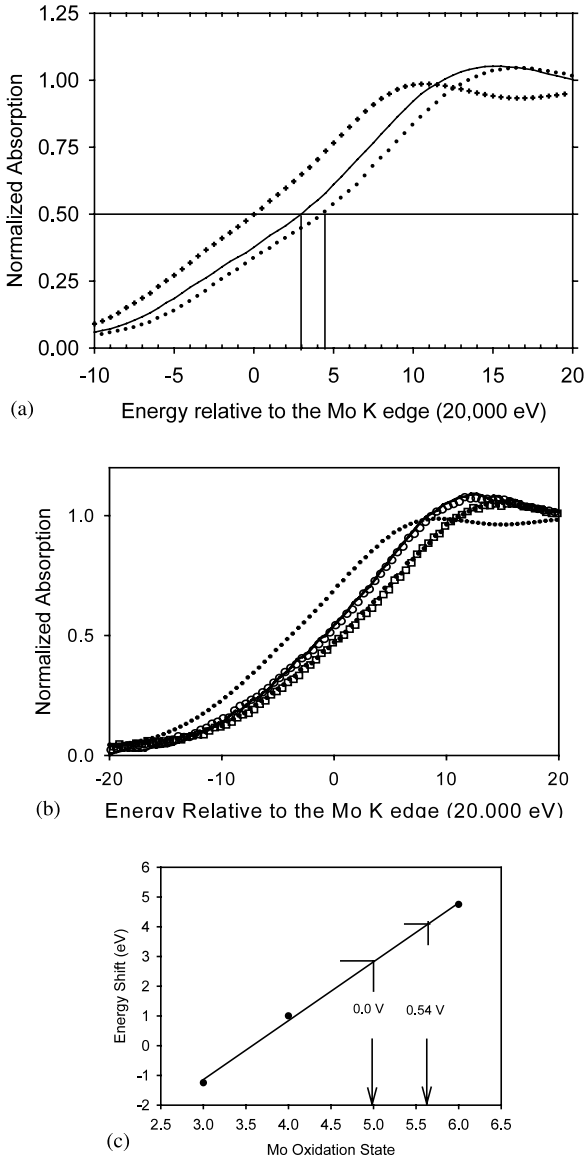

Fig. 12. XANES at the Mo K edge, (a) in 1 M $HClO_4$, (b) in 1 M $HClO_4$+0.3 M MeOH at 0.0 V (—), 0.24 V (○), 0.54 V (···) and 0.84 V (□) and (c) comparison of the oxidation state change between 0.54 and 0.84 V in 1 M $HClO_4$ using a standard curve. A standard curve for Mo foil (+) is shown for reference.

4. Discussion and summary

Results of this investigation point to significant improvements in CO tolerance with PtMo/C (3:1 a/o), which shows a two to 3-fold enhancement in performance compared to the current state of the art PtRu/C (1:1 a/o) at 85 °C with 100 ppm CO in H_2. However, the corresponding performance for direct MeOH oxidation is not true, wherein no enhancement is observed. Cyclic voltammograms show evidence of both Pt and Mo features and of a redox couple involving Mo. Voltammograms for CO stripping shows two distinct peaks. The first peak for CO oxidation occurs at very low potentials ($\sim$0.05 V) and corresponds to CO oxidation initiated by Mo alloyed to Pt. This is followed by CO stripping at 0.55 V, a potential akin to CO oxidation by Pt oxides. Voltammograms also show PtMo/C is very stable and there is no evidence of any Mo dissolution in the potential window of −50 mV to 1.2 V.

XANES and EXAFS analysis at the Pt L and Ru and Mo K edges confirm the nominal compositions and alloy formation especially for PtMo/C. The increase in the d-band vacancies and the lowering of the Pt–Pt bond distances occur for both the alloys, however, this effect is more significant for PtRu/C. Analysis of the spectrum shows that while there is a competition for sites on the Ru surface for oxide formation (by water activation) and CO, the Mo surface has no affinity for CO, and therefore, it is available for efficient CO removal especially at low overpotentials. CO adsorption occurs on the Pt surfaces on both PtRu/C and PtMo/C. At higher overpotentials, Pt oxides are formed on the PtMo/C ($\sim$0.8 V) which is not indicated in PtRu/C, wherein a shift in the onset of Pt–OH formation is detected. This explains the two distinct CO stripping peaks for PtMo/C in contrast to only one on PtRu/C. Therefore, as far as CO oxidation is concerned, Ru oxy-hydroxides play a principle role in PtRu/C in contrast to PtMo/C where both oxides on Mo (at low overpotentials) and Pt (at high overpotentials) are key. In the case

of MeOH oxidation, there seems to be continuous build up of C_1 oxide species on the PtMo/C in contrast to PtRu/C. This is in contrast to the situation during CO oxidation. Hence a more complicated interaction occurs in the PtMo case where the oxy-hydroxides of Mo are no longer able to oxidize the products of MeOH oxidation. Details of this mechanism are under investigation. The Mo K edge XANES spectra at 0.0 V shows that Mo is present as a hydrated oxide species with an approximate oxidation state of (+V), such as $MoO(OH)_2$. There is a change in the oxidation state of Mo beyond 0.54 V irrespective of the presence or absence of MeOH.

Acknowledgements

The authors gratefully acknowledge the support of the US Department of Energy, Division of Material Science, under contract number DE-FG05-89ER45384 for its role in the development and operation of beam line X11A at the NSLS. The NSLS is supported by the Department of Energy, Division of Material Science under contract number DE-AC02-98CH10886. The authors also acknowledge a subcontract from NASA-JPL for the investigation on the direct MeOH oxidation characteristics. Assistance in measurement of steady state kinetics for direct methanol oxidation on the electrocatalysts at NASA-JPL by C. Witham and S. R. Narayanan is gratefully acknowledged. Support from the ETEK division of Denora, NA (Somerset, NJ) is gratefully acknowledged for the investigations on CO tolerance on PtMo electrocatalysts. Support from the Department of Education under the auspices of a GAAN scholarship is acknowledged for supporting one of the graduate students (Richard C. Urian).

References

[1] T.D. Jarvi, E. Stuve, in: Electrocatalysis (Frontiers of Electrochemistry), P.N. Ross, J. Lipkowski (Eds.), Wiley, 1998, p. 400.
[2] S. Mukerjee, J. McBreen, J. Electrochem. Soc. 146 (2) (1999) 600.
[3] K. Wang, H.A. Gasteiger, N.M. Markovic, P.N. Ross, Electrochim. Acta 41 (1996) 2587.
[4] S. Mukerjee, S.J. Lee, E.A. Ticianelli, J. McBreen, B.N. Grgur, N.M. Markovic, P.N. Ross, J.R. Giallombardo, E.S. DeCastro, Electrochem. Solid State Lett. 2 (1999) 12.
[5] B.N. Grgur, N.M. Markovic, P.N. Ross, J. Electrochem. Soc. 146 (1999) 1613.
[6] B.N. Grgur, G. Zhuang, N.M. Markovic, P.N. Ross, Jr., J. Phys. Chem. B 101 (1997) 3910.
[7] B.N. Grgur, N.M. Markovic, P.N. Ross, Jr., J. Phys. Chem. B 102 (1998) 2494.
[8] M.C. Denis, P. Gouerec, D. Guay, J.P. Dodelet, G. Lalande, R. Schulz, J. Appl. Electrochem. 30 (2000) 1243.
[9] A. Pozio, L. Giorgi, E. Antolini, E. Passalacqua, Electrochim. Acta 46 (2000) 555.
[10] H. Zhang, Y. Wang, E.R. Fachini, C.R. Cabrera, Electrochem. Solid State Lett. 2 (1999) 437.
[11] R.C. Urian, S. Mukerjee, C. Witham, S. Narayanan, and T. Valdez, Extended Abstracts of the Electrochemical Society, Spring Meeting, 25–30 March 2001, Symposium on Direct Methanol Fuel Cells, 2001.
[12] S. Mukerjee, S. Srinivasan, J. McBreen, M.P. Soriaga, J. Electrochem. Soc. 142 (1995) 1409.
[13] S. Mukerjee, S. Srinivasan, J. McBreen, M.P. Soriaga, J. Phys. Chem. 99 (1995) 4577.
[14] S.J. Lee, S. Mukerjee, J. McBreen, Y.W. Rho, Y.T. Kho, T.H. Lee, Electrochim. Acta 43 (1998) 3693.
[15] C.K. Witham, W. Chun, T.I. Valdez, S.R. Narayanan, Electrochem. Solid State Lett. 3 (2000) 497.
[16] J. McBreen, S. Mukerjee, J. Electrochem. Soc. 142 (1995) 3399.
[17] J. McBreen, J. Electroanal. Chem. 357 (1993) 373.
[18] J. Wong, F.W. Lytle, R.P. Messmer, D.H. Maylotte, Phys. Rev. B: Condens. Matter 30 (1984) 5596.
[19] A.N. Mansour, J.W. Cook, Jr., D.E. Sayers, J. Phys. Chem. 88 (1984) 2330.
[20] A.N. Mansour, J.W. Cook, Jr., D.E. Sayers, R.J. Emrich, J.R. Katzer, J. Catal. 89 (1984) 462.
[21] J.B.A.D. Van Zon, D.C. Koningsberger, H.F.J. Van't Blik, D.E. Sayers, J. Chem. Phys. 82 (1985) 5742.
[22] F.B.M. Duivenvoorden, D.C. Koningsberger, Y.S. Uh, B.C. Gates, J. Am. Chem. Soc. 108 (1986) 6254.
[23] R.E. Benfield, J. Chem. Soc. Faraday Trans. 88 (1992) 1107.
[24] S. Mukerjee, J. McBreen, J. Electrochem. Soc. 143 (1996) 2285.
[25] W. Vogel, J. Lundquist, P.N. Ross, Jr., P. Stonehart, J. Electrochem. Soc. 133 (1986) 1574.
[26] S.J. Lee, S. Mukerjee, E.A. Ticianelli, J. McBreen, Electrochim. Acta 44 (1999) 3283.
[27] J.J. Rehr, J.M.d.L., S.I. Zabinski, R.C. Albers, J. Am. Chem. Soc. 113 (1991) 5135.
[28] M. Krausa, W. Vielstich, J. Electroanal. Chem. 379 (1994) 307.
[29] C.P. Wilde, M. Zhang, Electrochim. Acta 39 (1994) 347.
[30] S. Mukerjee, J. McBreen, Proc.-Electrochem. Soc., PV- 97-13 (1997) (Electrode Materials and Processes for Energy Conversion and Storage IV): p. 36–51.
[31] H.A. Gasteiger, N.M. Markovic, P.N. Ross, Jr., J. Phys. Chem. 99 (1995) 8290.